Direct and indirect excitation mechanisms in two-photon photoemission spectroscopy of Cu(111) and CO/Cu(111)

M. Wolf, A. Hotzel, E. Knoesel, and D. Velic
Fritz-Haber-Institut der Max-Planck-Gesellschaft, Faradayweg 4-6, D-14195 Berlin, Germany
(Received 1 September 1998)

It is demonstrated that the dependence of the two-photon photoemission (2PPE) yield on the polarization of the exciting laser light provides detailed information about the excitation mechanism and the orientation of transition dipole moments in the 2PPE process. In particular, it is possible to distinguish between a *direct* two-photon excitation process, where both electronic transitions are induced by the electric fields at the surface, and an *indirect* mechanism, where the first excitation step occurs in the substrate. In the latter process the intermediate state in 2PPE is populated by scattering of photoexcited hot electrons from the substrate, which are subsequently photoemitted by the second laser pulse. The analysis is applied to 2PPE from clean and CO covered Cu(111). Furthermore, we have derived analytical expressions for the 2PPE signal based on the optical Bloch equations for a three-level system excited with continuous light beams. They allow us to calculate 2PPE spectra of surface states for a variety of cases. [S0163-1829(99)02008-1]

I. INTRODUCTION

Two-photon photoemission (2PPE) spectroscopy is a powerful experimental technique to investigate the surface electronic structure as well as the dynamics of electrons in normally unoccupied electronic states at surfaces.[1–11] Early studies on 2PPE from surfaces have focused on the electron dynamics of semiconductors[1,2] and spectroscopy of image potential states on metals.[3,4] More recent developments in ultrafast laser techniques have opened a rapidly growing research field, where 2PPE has been used with great success to study the electron dynamics in adsorbate overlayers,[5,6] coherent excitation of electron wave packets,[7] optical dephasing, and phase control of electrons in metals,[8,9] phonon contributions to the surface state dynamics,[10] and spin-resolved electron relaxation in ferromagnetic systems.[11]

However, in many cases little is known about the excitation mechanism and the transition probabilities in two-photon photoemission. In 2PPE a first (pump) laser pulse excites the sample (resulting in the population of normally unoccupied electronic states) followed by excitation to a final state above the vacuum level by a second (probe) laser pulse. Figure 1 schematically illustrates different excitation pathways in 2PPE. Photoemission can be induced either by a sequence of *direct* electronic transitions from the initial state $|i\rangle$ to the final state $|f\rangle$, or by an *indirect* process in which the intermediate state $|k\rangle$ is populated by scattering and relaxation of ''hot'' electrons, which are photoexcited in the substrate. For example, in 2PPE from a Cu(111) [or Ag(111)] surface the first $(n=1)$ image potential state may be populated either by direct excitation from the occupied $(n=0)$ surface state at the center of the surface Brillouin zone (at $k_{\|}=0$)[10,12] or via scattering of ''hot'' substrate electrons into the image state.[12] The direct excitation process dominates if the pump-photon energy is close to the energy difference between the $(n=0)$ and $(n=1)$ state.[10,12]

The direct and indirect excitation mechanisms differ in the role of coherence (the phase relation between the photoexcited electron and its photohole) in the 2PPE process. For the indirect mechanism the coherence of the excitation is lost by phase-breaking scattering events and the 2PPE process can be separated into two subsequent steps. Coherent control schemes, which rely on the phase relation between pump and probe pulses, are not applicable.[8] For a direct excitation process the transition rates between individual levels are given by the transition dipole moments and the electric fields at the surface. Within the optical dephasing times of the transitions the electron dynamics can be controlled by the phase of the electric fields.[7,8] The time evolution of the 2PPE signal can be calculated using optical Bloch equations, which fully describe the coherent dynamics as well as the energy and phase relaxation in the system.[7,8,10,12,13] This treatment has been applied to 2PPE from image potential states. The σ symmetry of these states implies that the transition dipole moments are oriented along the surface normal, and thus 2PPE is in-

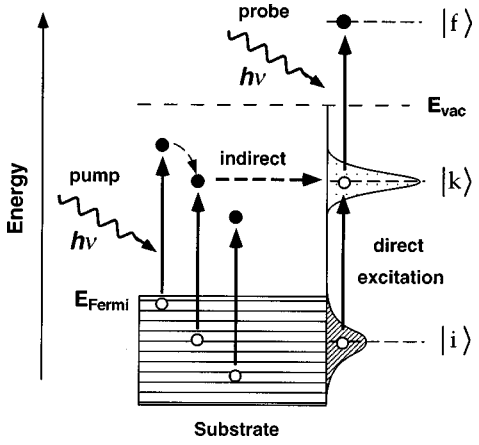

FIG. 1. Direct vs indirect excitation mechanism in pump-probe two-photon photoemission. For direct excitation the transition rates between the levels $|i\rangle$, $|k\rangle$, and $|f\rangle$ are given by the transition-dipole moments and the electric fields at the surface. In the indirect process the first photon is absorbed in the substrate followed by scattering of a photoexcited electron into the intermediate state $|k\rangle$.

duced by the normal component of the electric field.

In this paper we derive some analytical expressions for the 2PPE signal by solving the optical Bloch equations for a three-level system under continuous wave (cw) excitation. The 2PPE intensity is proportional to a term that determines the line shape and peak intensities in 2PPE spectroscopy, and to a term that depends on the polarization of the laser light (see the Appendix). Here we focus on the polarization dependence of the 2PPE signal from electronic states on clean and carbon monoxide (CO) covered Cu(111) with various symmetries. We show that it is possible to discriminate between a *direct* two-photon excitation process and an *indirect* (i.e., substrate mediated) excitation mechanism in 2PPE as illustrated in Fig. 1. Related studies using polarized light have been performed to elucidate the excitation mechanism in surface photochemistry.[14–17] Our analysis also allows us to draw conclusions about the orientation of the transition dipole moments in the 2PPE process.

The system CO/Cu(111) was chosen because the 2PPE spectra show for the $(\sqrt{3}\times\sqrt{3})$R30° phase pronounced features from the Cu *d* band as well as adsorbate induced states with σ and π symmetry.[18] This allows us to analyze simultaneously the polarization dependence of several states with different symmetry. In a previous paper on 2PPE from CO/Cu(111) the unoccupied CO $2\pi^*$ derived resonance has been identified at 3.35 eV above the Fermi level.[19] Time-resolved photoemission studies have established an upper limit of 5 fs for the lifetime of the $2\pi^*$ level.[20,21] Recently, the manipulation of individual CO molecules on Cu(111) in scanning tunneling microscopy was found to be induced by the transient population of the CO $2\pi^*$ level by tunneling electrons from the STM tip.[21]

II. POLARIZATION DEPENDENCE OF THE 2PPE INTENSITY

In a direct two-photon photoemission process the pump pulse induces a direct electronic transition from an occupied initial state $|i\rangle$ to a normally unoccupied intermediate state $|k\rangle$; subsequently the electron is excited by the probe pulse to a final state $|f\rangle$ above the vacuum level, where it leaves the surface (see Fig. 1). This final state can be regarded as an ''inverse low-energy electron diffraction (LEED) state'' as in a one-photon photoemission theory.[22] In the following we consider equal pump and probe pulses, which induce an electric field $\mathrm{Re}[E_{\mathrm{inc}}(t)e^{-i\omega t}\cdot\mathbf{e}]$ at the surface; here $E_{\mathrm{inc}}(t)$ is the electric-field envelope of the incident laser pulse with center frequency ω and $\mathbf{e}$ is the normalized electric field at the surface. The two-photon transition rate to the final state, W_{if}, which depends on the energy- and phase-relaxation rates and on the transition matrix elements between the states $|i\rangle$, $|k\rangle$, and $|f\rangle$, can be calculated by solving the optical Bloch equations for a three-level system.[10] For the case of cw beams $[E_{\mathrm{inc}}(t)=\mathrm{const}]$ we have derived an analytical solution, which is given in the Appendix. Within the dipole approximation the dependence of the 2PPE signal on the polarization vector is given in the case of one discrete intermediate state $|k\rangle$ by [see Eq. (A10)]:

$$W_{if}\propto|(\boldsymbol{\mu}_{ik}\cdot\mathbf{e})(\boldsymbol{\mu}_{kf}\cdot\mathbf{e})|^2. \tag{1.1}$$

Here $\boldsymbol{\mu}_{ik}$ and $\boldsymbol{\mu}_{kf}$ denote the transition-dipole moments between the electronic states $|i\rangle$, $|k\rangle$, and $|f\rangle$. Throughout this paper, we only consider *real* transition-dipole moments. By exploiting the symmetry of the electronic states this expression can be simplified. In this paper, we study 2PPE along the surface normal, therefore the final state is totally symmetric for all relevant point groups. If, for example, the initial and intermediate states have σ symmetry, the transition-dipole moments are oriented along the surface normal (defined as the *z* direction), and thus $W_{if}\propto(\mu_{ik}{}^z\mu_{kf}{}^z)^2|e_z|^4$. The latter expression is obviously totally symmetric for all relevant point groups. In general, the transition-dipole moments may be arbitrarily tilted with respect to the surface normal and may have nonvanishing components in the surface plane. However, the resulting 2PPE signal (for normal emission) must be invariant under the symmetry operations of the surface-point group. In order to obtain a symmetrized expression for W_{if}, we project the electric field $\mathbf{e}$ onto the transition moments $\boldsymbol{\mu}_{ik}$ and $\boldsymbol{\mu}_{kf}$ and calculate [see Eq. (A12)]:

$$W_{if}\propto\left|\sum_{\mathrm{sym}}(\boldsymbol{\mu}_{ik}\cdot\mathbf{e})(\boldsymbol{\mu}_{kf}\cdot\mathbf{e})\right|^2, \tag{1.2}$$

where Σ_{sym} denotes the sum over the different contributions to W_{if} obtained by applying the symmetry operations of the surface point group simultaneously to $\boldsymbol{\mu}_{ik}$ and $\boldsymbol{\mu}_{kf}$. This expression is applicable in the case of several intermediate states $|k\rangle$, which are degenerate for symmetry reasons [see the Appendix, Eq. (A12)]. Note that in a direct two-photon process excitation of real and virtual intermediate states may contribute to the signal.[23] On the other hand, if the 2PPE signal originates from different domains on the surface or from noninteracting initial states one has to average over the *signal intensities* according to the symmetry of the surface [see Eq. (A13)]:

$$W\propto\sum_{\mathrm{sym}}|(\boldsymbol{\mu}_{ik}\cdot\mathbf{e})(\boldsymbol{\mu}_{kf}\cdot\mathbf{e})|^2. \tag{1.3}$$

To calculate the polarization dependence of W the normalized electric field $\mathbf{e}$ at the surface must be known. Using the Fresnel equations, the components e_x, e_y, and e_z of the electric field on the vacuum side can be obtained for an abrupt interface where the complex refractive index is represented by a step function:[14,15,24]

$$\begin{aligned} e_x&=(1-r_p)\cos\Theta_i\cos\Phi,\\ e_y&=(1+r_s)\sin\Phi,\\ e_z&=(1+r_p)\sin\Theta_i\cos\Phi. \end{aligned} \tag{2}$$

Here, Θ_i is the angle of incidence with respect to the surface normal, Φ is the polarization angle of the light with respect to the plane of incidence (defined as the *x*-*z* plane) as illustrated in Fig. 2. The coefficients r_p and r_s, which depend on the complex refractive index $n+ik$ and on the angle of incidence, are the Fresnel reflection coefficients for *p*-polarized ($\Phi=0°$) and *s*-polarized ($\Phi=90°$) light, respectively.[24] Using the optical constants for copper [$n=1.35$, $k=1.71$ at $h\nu=4.03$ eV (Ref. 25)], we calculate for the electric fields on

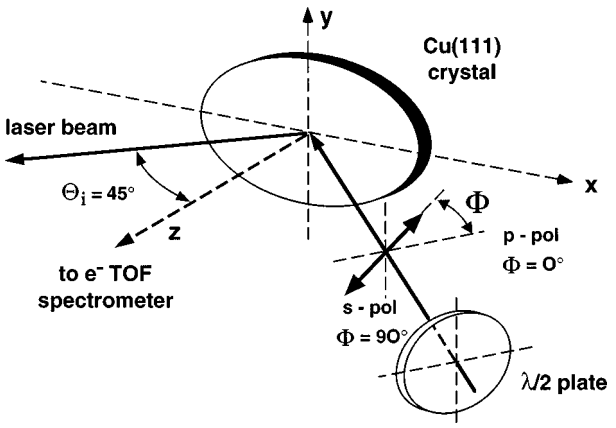

FIG. 2. Schematic overview of the experimental geometry: The *p*-polarized laser beam passes a half wave (λ/2) plate and is incident (in the *x*-*z* plane) on the Cu(111) surface under 45° from the surface normal (the *z* axis). The 2PPE signal of photoemitted electrons is detected along the surface normal as a function of the polarization angle ϕ, which is changed by rotating the λ/2 plate.

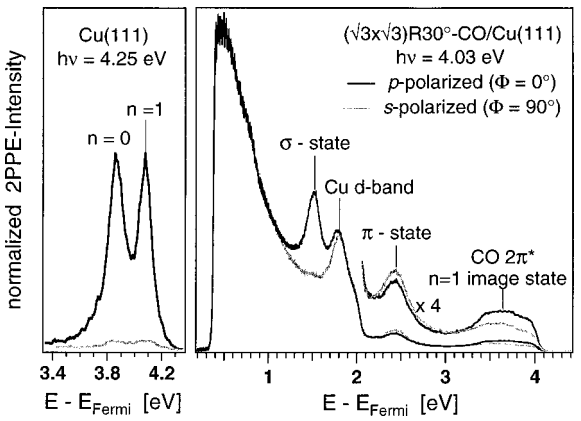

FIG. 3. 2PPE spectra recorded with *s*- and *p*-polarized light for clean Cu(111) (left) and for a $(\sqrt{3}\times\sqrt{3})$R30°-CO layer on Cu(111) (right). The energy axes give the intermediate state energies. The spectra are normalized to match the 2PPE intensities at low energies, where the signal is dominated by secondary electrons.

the vacuum side $e_x = 0.533 - i0.308$ and $e_z = 0.882 + i0.308$ for *p* polarization ($\Phi = 0°$) and $e_y = 0.389 - i0.356$ for *s* polarization ($\Phi = 90°$) at $\Theta_i = 45°$ angle of incidence.[24]

This classical treatment provides a useful description of the parallel field components e_x and e_y, which are continuous across the interface, but results in unphysical perpendicular field components due to the abrupt change at the interface.[26,27] The strong spatial variations of the perpendicular fields may invalidate the dipole approximation.[27] However, calculations of the local electric fields for a jellium model show that deviations from the classical Fresnel theory are only relevant if the photon energy is comparable to the bulk-plasmon energy.[26] In 2PPE typical photon energies are small compared to the bulk plasmon energy (which is 10 eV for Cu). One simple improvement to the classical theory is to introduce an effective refractive index $n_0 < n_{\text{eff}} < n_1$, which varies smoothly across the interface from its value $n_0 = 1$ on the vacuum side to $n_1 = n + ik$ in the bulk.[14,15] In this approximation the intensity of the electric field perpendicular to the surface is $e_z^2/|n_{\text{eff}}|^2$.

Next we consider the indirect excitation mechanism in Fig. 1, where the intermediate state $|k\rangle$ is populated via scattering of photoexcited electrons from the substrate. This process is similar to the substrate-mediated excitation mechanism in surface photochemistry induced by hot electron attachment to unoccupied adsorbate resonances.[28] In the first approximation the population of the intermediate state is proportional to the substrate absorbance.[14] In the second step of the 2PPE process the electron is excited by the probe pulse to the final state $|f\rangle$ with a transition rate given by Fermi's golden rule $W_{kf} \propto |(\boldsymbol{\mu}_{kf} \cdot \mathbf{e})|^2$, and hence the polarization dependence of the 2PPE signal is given by

$$W \propto (A_p \cos^2 \Phi + A_s \sin^2 \Phi) |\boldsymbol{\mu}_{kf} \cdot \mathbf{e}|^2. \tag{3}$$

Here, $A_p = (1 - |r_p|^2)$ and $A_s = (1 - |r_s|^2)$ denote the substrate absorbance for *p*- and *s*-polarized light, respectively, and Φ is the angle of the polarization (see Fig. 2). For copper we calculate an absorbance of $A_p = 0.75$ ($A_s = 0.5$) for *p*-polarized (*s*-polarized) light incident at $\Theta_i = 45°$. For non-vanishing components of $\boldsymbol{\mu}_{kf}$ within the surface plane the transition rate in Eq. (3) must be averaged according to the symmetry of the surface.

III. EXPERIMENT

The experiments were performed in a UHV chamber equipped with an electron time-of-flight spectrometer for 2PPE spectroscopy as described elsewhere.[10] Femtosecond laser pulses are generated by a 200-kHz Ti Sapphire laser system pumping an optical parametric amplifier (OPA). The visible OPA output is frequency doubled to generate 70-fs pulses with photon energies of $h\nu = 4 - 4.3$ eV. The *p*-polarized laser beam passes a half wave (λ/2) plate and is incident on the Cu(111) sample under 45° with respect to the surface normal (the *z* axis), as schematically shown in Fig. 2. For *p* polarization (*s* polarization) the electric field is parallel (perpendicular) to the plane of incidence (the *x*-*z* plane). Analysis of the LEED pattern indicates that the *x* axis is rotated by 15° with respect to the $[\bar{1}10]$ direction of the Cu(111) surface. In the experiment the polarization angle Φ is varied by rotation of the λ/2 plate around the axis defined by the laser beam. The Cu(111) crystal is cleaned by standard procedures. CO is dosed at 88 K up to saturation coverage, resulting in a (1.4×1.4) LEED pattern; subsequent annealing to 117 K leads to a CO $(\sqrt{3}\times\sqrt{3})$R30° phase, as described previously (see Ref. 29 and references therein). All 2PPE spectra are recorded for emission along the surface normal (i.e., for an electron wave-vector component parallel to the surface $k_\parallel = 0$).

IV. RESULTS AND DISCUSSION

Figure 3 displays 2PPE spectra recorded with *p*- and *s*-polarized light for a clean Cu(111) surface (left panel, $h\nu = 4.25$ eV) and a $(\sqrt{3}\times\sqrt{3})$R30°-CO layer on Cu(111) (right panel, $h\nu = 4.03$ eV). The spectra are plotted vs intermediate state energy, i.e., measured kinetic energy plus work function minus once the photon energy. The two peaks on clean Cu(111) originate from the occupied ($n = 0$) surface state and the first ($n = 1$) image potential state at $k_\parallel = 0$.[10,30] Both

states are observed only with *p*-polarized light (the small 2PPE signal observed for *s* polarization is attributed to imperfect polarization). The spectra for CO/Cu(111) show pronounced structures from the Cu *d* band, as well as from adsorbate induced states. Analysis of the dependence of peak positions on the photon energy clearly reveals that all CO-induced peaks (labeled as σ, π, and $2\pi^*$ state) originate from normally unoccupied states.[18] Their binding energies are 1.45, 2.4, and 3.6 eV above E_F for the σ, π, and $2\pi^*$ state, respectively. The CO $2\pi^*$ state appears in 2PPE at all CO coverages, whereas the σ and π states are observed only for a well-ordered $(\sqrt{3}\times\sqrt{3})$R30° structure. In this context, the denotation of the two states as π and $2\pi^*$ state simply means that these states are also observed with *s*-polarized light (in contrast to the σ state, which is only observed with *p*-polarized light). It does not imply that these states have strict π symmetry, as will be discussed below. While the $2\pi^*$ state is derived from the unoccupied $2\pi^*$ orbitals of the free CO molecule[18–21] the σ state and the π state are believed to originate from a folding of Cu bands in the reduced-surface Brioullin zone due to the $(\sqrt{3}\times\sqrt{3})$ overlayer structure.[18] This is consistent with the fact that the latter states are only observed for the well-ordered $(\sqrt{3}\times\sqrt{3})$ structure. Further details of the unoccupied electronic structure of the CO/Cu(111) system will be discussed elsewhere.[18]

The spectra for *p*- and *s*-polarized light have been normalized to equal intensities at low energies, where the 2PPE signal is dominated by secondary electrons ($E-E_F<1.2$ eV in Fig. 3, right panel). These secondary electrons originate from photoabsorption in the bulk followed by inelastic scattering and relaxation processes. On Cu(111) the existence of a band gap at $k_\parallel=0$ implies that such scattering processes occur both in the intermediate and the final state (at $k_\parallel\neq 0$) considering the observed long lifetimes and the intensity of secondary electrons in the 2PPE spectra.[31] The 2PPE signal at low energies is, therefore, assumed to be proportional to the substrate absorbance in both excitation steps [i.e., $\propto A_\Phi{}^2=(A_p\cos^2\Phi+A_s\sin^2\Phi)^2$]. Throughout this paper all 2PPE spectra are normalized to the secondary-electron intensity at low energies. For a 2PPE process where both excitation steps are driven by photoabsorption in the substrate, this normalization procedure would result in a *constant* normalized intensity as a function of the polarization angle Φ. Any remaining polarization dependence will then indicate the contribution from a direct excitation process in at least one of the excitation steps in 2PPE.

Figure 4 compares the polarization dependence of the normalized 2PPE intensities from (a) the $(n=0)$ surface state and the $(n=1)$ image potential state on clean Cu(111) ($h\nu=4.03$ eV and 4.25 eV) and (b) of the σ state of the CO $(\sqrt{3}\times\sqrt{3})$ phase ($h\nu=4.03$ eV). For the σ state the secondary electron background has been subtracted (see Fig. 3). For all these states the intensity is maximal for *p* polarization and vanishes for *s*-polarized light as expected for states with σ symmetry. When the polarization angle Φ is scanned between *p* and *s* polarization we find that the $(n=0)$ and $(n=1)$ states behave identically and that their intensities are nicely fitted by $W\propto|e_z|^4$ [solid line in Fig. 4(a)]. This reveals that 2PPE from the $(n=0)$ and $(n=1)$ states at these photon

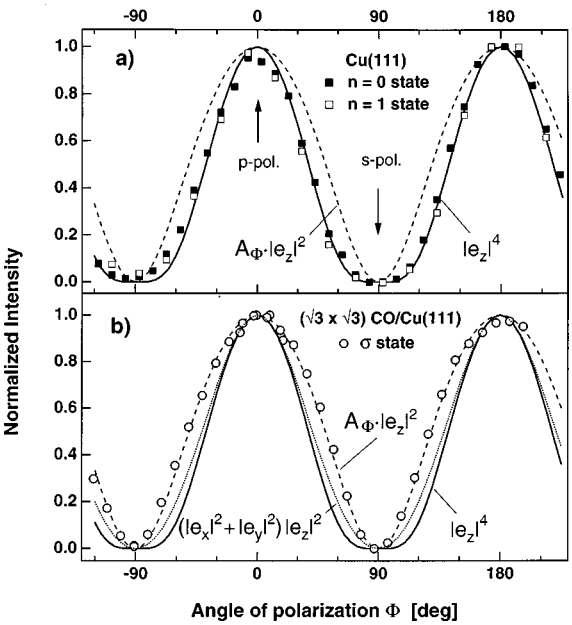

FIG. 4. (a) Dependence of the 2PPE signal from the $n=0$ surface state and the $n=1$ image potential state on clean Cu(111) on the polarization angle ϕ (defined in Fig. 2). (b) Same for the σ state of the $(\sqrt{3}\times\sqrt{3})$CO/Cu(111) phase. The dashed lines correspond to an indirect mechanism, where the primary excitation step occurs in the substrate and is governed by the absorbance $A_\Phi=A_p\cos^2\Phi+A_s\sin^2\Phi$. The solid and dotted lines show the prediction for a direct two-photon process induced by e_z^4 and $(e_x^2+e_y^2)e_z^2$, respectively.

energies is induced by a *direct* two-photon excitation mechanism with the transition dipole moments oriented along the surface normal in *both* excitation steps (i.e., $\mu_{ik}{}^x=\mu_{ik}{}^y=\mu_{kf}{}^x=\mu_{kf}{}^y=0$). This scenario is consistent with the photon-energy dependence of the lineshapes and intensities of the $(n=0)$ and $(n=1)$ states as discussed in the Appendix (see Fig. 6). Consistent results were also obtained in bichromatic 2PPE experiments, where the polarization vectors of the pump and probe pulses were varied independently (not shown). On the other hand, the intensity of the CO-induced σ state in Fig. 4(b) shows a polarization dependence that is clearly different from that of the $(n=0)$ and $(n=1)$ states. It can be fitted by $W\propto A_\Phi\cdot|e_z|^2$ according to Eq. (3) with $\mu_{kf}{}^x=\mu_{kf}{}^y=0$ [see dashed line in Fig. 4(b)]. This indicates an *indirect* excitation process where the primary absorption step lies in the substrate (see Fig. 1). A direct excitation of the σ state from an initial state (e.g., from the Cu *d* bands) with a dipole moment in the surface plane would exhibit a polarization dependence like $W_{if}\propto(|e_x|^2+|e_y|^2)\cdot|e_z|^2$ and can be clearly ruled out [see dotted line in Fig. 4(b)].

To rationalize the dominance of the indirect (substrate mediated) excitation mechanism observed for the σ state, we note that this state appears in the 2PPE spectra at lower energies than the *d*-band peak (see Fig. 3). The σ state can thus be populated by secondary electrons resulting from *d*-band excitations in copper. Such secondary processes can involve either the decay from higher-lying states (above E_F) or the relaxation of photogenerated holes in the Cu *d* band (~2 eV below E_F) which leads to the generation of Auger

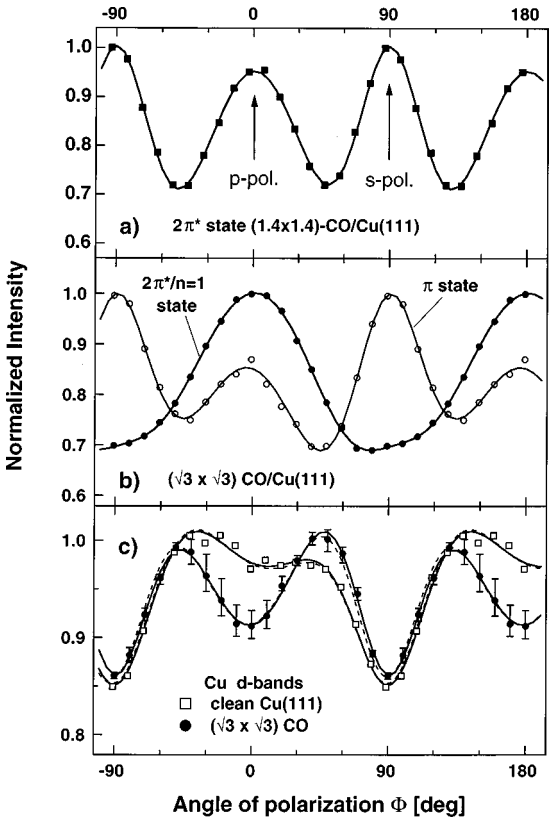

FIG. 5. Polarization dependence of the 2PPE signal of (a) the $2\pi^*$ level at CO saturation (1.4×1.4) coverage, (b) the π and $2\pi^*$ states on ($\sqrt{3}\times\sqrt{3}$)-CO/Cu(111), and (c) the Cu *d*-band peak on clean Cu(111) and ($\sqrt{3}\times\sqrt{3}$)-CO/Cu(111), respectively. The solid and dashed lines are fits of Eqs. (1.2) and (1.3) to the data (see text). Note that the $2\pi^*$ level on ($\sqrt{3}\times\sqrt{3}$)-CO overlaps with the $n=1$ image state, which has σ symmetry.

electrons.[31] These secondary electrons exhibit relatively long inelastic lifetimes, and thus have correspondingly long mean-free-path lengths. Excited state population by secondary electrons in 2PPE (similar to substrate mediated excitation in surface photochemistry[28]) may, therefore, be more efficient compared to a direct excitation mechanism.

We now discuss the polarization dependence of the CO-induced $2\pi^*$ and π state, and the *d*-band peak [see Figs. 5(a)–5(c)]. Note the differences compared to states with σ symmetry (Fig. 4). First, we can rule out a substrate-mediated excitation mechanism; fits to Eq. (3) show that it is impossible to explain the data in Fig. 5 by an indirect excitation process for *any* orientation of the dipole moment $\boldsymbol{\mu}_{kf}$ in Eq. (3) even when background subtraction is allowed. Hence, direct excitation in both steps of the 2PPE process must be dominant. The solid lines in Fig. 5 show fits to the polarization data for a *direct* excitation mechanism without any background correction. Herein, we have used Eq. (1.2), which has been symmetrized according to the C_{3v} symmetry of the Cu(111) surface (three mirror planes and rotations around the surface normal by 120°). In general, we find for all π states and the Cu *d* bands that the transitions dipole moments must have nonvanishing components in the surface plane but have different orientations in both excitation steps.

For the CO $2\pi^*$ state at saturation coverage we obtain from the fits [solid line, Fig. 5(a)] that the transition-dipole moments $\boldsymbol{\mu}_{ik}$ and $\boldsymbol{\mu}_{kf}$ are tilted by $\Theta_{ik}=\Theta_{kf}=61°$ from the surface normal and rotated within the surface plane (azimuthal angle) by $\Phi_{ik}=19.5°$ and $\Phi_{kf}=100°$ with respect to the plane of incidence. This means that the components in the surface plane are oriented almost perpendicular to each other in the two excitation steps ($\Phi_{kf}-\Phi_{ik}\sim80°$). The corresponding numbers for the ($\sqrt{3}\times\sqrt{3}$)-CO coverage [Fig. 5(b)] are $\Theta_{ik}=56°$, $\Theta_{kf}=55°$, $\Phi_{ik}=16°$, and $\Phi_{kf}=102°$ for the $2\pi^*$ state and $\Theta_{ik}=60°$, $\Theta_{kf}=61°$, $\Phi_{ik}=17.6°$, and $\Phi_{kf}=102°$ for the π state, respectively. Note that the polarization dependence of the CO-induced $2\pi^*$ and π states cannot be fitted using Eq. (13). For both states we find nonvanishing normal components $\mu_{kf}{}^z\neq0$. For a *free* (noninteracting) CO molecule oriented perpendicular to the surface the transition moment for excitation from the $2\pi^*$ orbital to a final state, which is totally symmetric must be orthogonal to the molecular axis (i.e., $\mu_{kf}{}^z=0$). Since in the ($\sqrt{3}\times\sqrt{3}$) overstructure the CO molecule *is* oriented perpendicular to the surface,[29] the nonvanishing components $\mu_{kf}{}^z\neq0$ mean that neither the π state nor the $2\pi^*$ state have strict π symmetry. In the case of the $2\pi^*$ state, this is attributed to hybridization of the CO $2\pi^*$ states with the copper substrate. As was mentioned above, the π state is believed to have mainly copper character.

The exact angles of the transition-dipole moments of the $2\pi^*$ and the π state depend somewhat on the model, e.g., on whether a background is subtracted, and on the fact that the relevant electric field is identified with the field on the *vacuum* side [Eq. (2)]. However, it is impossible to fit the polarization dependence curves of Fig. 5 with vanishing $\mu_{kf}{}^z$ components. Interestingly, we find that the polarization dependence of the CO $2\pi^*$ state in the ($\sqrt{3}\times\sqrt{3}$)-CO structure [Fig. 5(b)] is different compared to saturation coverage [Fig. 5(a)]. In the ($\sqrt{3}\times\sqrt{3}$) structure the normal components of the transition dipole moments are about 15% stronger, indicating an additional contribution from a state with σ symmetry. We attribute this to overlapping peaks of the CO $2\pi^*$ state with the $n=1$ image-potential state in the 2PPE spectrum at the ($\sqrt{3}\times\sqrt{3}$) coverage. This assignment is backed up by angle-resolved 2PPE measurements for the ($\sqrt{3}\times\sqrt{3}$)R30°-CO/Cu(111) phase, where we observe that the 2PPE feature at E-$E_F=3.6$ eV in Fig. 3 shows a clear upward dispersion for the σ-symmetry state (assigned to the $n=1$ image-potential state) and a weak downward dispersion for the CO $2\pi^*$ state.[18] Compared to clean Cu(111) the image state is shifted towards the Fermi level due to a lowering of the work function by 0.5 eV, and its linewidth is considerably broader. A similar persistence of an image state upon CO adsorption was reported by Tsuei and Johnson for an ordered $c(2\times2)$-CO layer on Cu(100).[32] In this case the image state was also found to overlap with the CO $2\pi^*$ resonance. Very recently, Reuß and co-workers carried out a detailed time-resolved 2PPE study of the influence of CO adsorption on the dynamics of image state on Cu(100).[33] They found a pronounced increase of the ''pure'' dephasing rates (see the Appendix) upon CO adsorption. As shown in the Appendix, ''pure'' dephasing can lead to the population of an intermediate state by direct excitation, even if the transition from the initial state is not in resonance with the pump-photon energy.[12] This might explain the fact that the

$2\pi^*$ state (and also the $n=1$ image state on the $(\sqrt{3}\times\sqrt{3})$ coverage) is excited directly in 2PPE with $h\nu=4.03$ eV photon energy, although the copper bulk-band structure has a band gap in the (111) direction above $E\text{-}E_F=-0.85$ eV.

Figure 5(c) compares the polarization dependence of the Cu *d*-band peak on clean Cu(111) and $(\sqrt{3}\times\sqrt{3})$-CO/Cu(111). On the clean surface, the 2PPE signal from the *d* band is clearly asymmetric around $\Phi=0°$. This is attributed to the fact that the plane of incidence does not coincide with a mirror plane of the Cu(111) surface (i.e., the $[\bar{1}10]$ direction of the crystal is rotated by 15° with respect to the *x* axis in Fig. 2). A fit to Eq. (1.2) yields $\Theta_{ik}=48°$, $\Theta_{kf}=58°$, $\Phi_{ik}=12°$, and $\Phi_{kf}=121°$. Adsorption of the CO $(\sqrt{3}\times\sqrt{3})$ structure leads to a reduction of the normalized 2PPE signal around $\Phi=0°$ (*p* polarization) but no changes for *s*-polarized light ($\Phi=90°$); this effect is even more pronounced for the saturation coverage (not shown). Analysis by Eq. (1.2) indicates slightly smaller normal components of the transition-dipole moments for the CO-covered surface ($\Theta_{ik}=48°$, $\Theta_{kf}=60°$, $\Phi_{ik}=14°$, and $\Phi_{kf}=125°$). The 2PPE signal of the *d*-band peak originates from two-photon transitions via the projected band gap on Cu(111), and therefore off-resonant excitation of the image-potential state will contribute to the signal. The latter contribution will be reduced if the image-state lifetime ($\tau\sim 1/\Gamma_k$) becomes shorter upon CO adsorption [see the Appendix, Eq. (A11) for increasing Γ_k]. Finally, we note that the polarization data in Fig. 5(c) can also be fitted by Eq. (1.3) (see dashed lines); however, in this case 80% of the intensity must be subtracted as a background contribution. We thus believe that several intermediate states contribute to 2PPE from the Cu *d* band as described by Eqs. (1.2) and (A12).

In summary, we have developed a simple experimental approach to analyze the excitation mechanism in two-photon photoemission using polarized light. It allows us to discriminate between direct two-photon excitation mechanisms and indirect (substrate mediated) mechanisms, where the intermediate state in 2PPE is populated by photogenerated hot electrons from the substrate. In 2PPE from Cu(111) and CO/Cu(111) both processes were found. The substrate mediated mechanism observed for the σ state on the $(\sqrt{3}\times\sqrt{3})$R30°-CO surface is attributed to population by secondary electrons resulting presumably from *d*-band excitations in the substrate. In all other cases that we investigated in this paper, the direct excitation process prevails. For 2PPE from the CO-induced unoccupied electronic states labeled as $2\pi^*$ and π state the transition-dipole moments were found to have different orientations in the first- and second-excitation step. Such detailed insights into the excitation process would not be possible if only *s*- and *p*-polarized light were used for symmetry analysis. We note that with identical pump and probe pulses it is not possible to distinguish between the first- and the second-transition dipole moment in the 2PPE process ($\boldsymbol{\mu}_{ik}$ and $\boldsymbol{\mu}_{kf}$). However, this distinction can be made in bichromatic 2PPE experiments, which for the $(n=0)$ and $(n=1)$ states of the bare Cu(111) surface gave results that are consistent with monochromatic 2PPE.

Furthermore, we have derived analytical expressions for the 2PPE spectrum in a variety of cases of direct excitation. Our expressions, based on the optical Bloch equations, allow us to determine the influence of energy relaxation, ''pure'' dephasing, and the pump-photon energy on the lineshapes and intensities of ''initial state'' and ''intermediate state'' peaks in 2PPE. For the occupied surface state and the first-image potential state on Cu(111), a good agreement between the measured and calculated spectra and resonance curves was demonstrated.

ACKNOWLEDGMENTS

The authors would like to thank G. Ertl for generous support. We thank Th. Fauster for sharing his results prior to publication.

APPENDIX

In this appendix we derive some expressions for 2PPE in the case of *direct* excitation (where scattering and relaxation of hot substrate electrons is not involved). The expressions are based on the optical Bloch equations for a three-level system. A more general treatment can be found in Ref. 34. Here we only discuss 2PPE with cw beams. A lot of information can also be gained by solving the corresponding equations for femtosecond laser pulses,[10,12] but to our knowledge, in the general case this can only be done numerically.

A. 2PPE from one initial state, one intermediate state

First we consider the simplest case of a discrete initial state and a discrete intermediate state. This scenario applies, e.g., to the Cu(111) surface, where both the occupied surface state $n=0$ and the first (unoccupied) image potential state $n=1$ lie in the sp band gap in the (111) direction of Cu. This situation is described by a system consisting of an initial state $|i\rangle$, an intermediate state $|k\rangle$, and a continuum of final states $|f\rangle$ (f is an index variable), which are identified with the states of the free electron in the vacuum. These states are eigenstates of the unperturbed Hamiltonian H_0 with $H_0|i\rangle=E_i|i\rangle=\hbar\omega_i|i\rangle$, etc. We assume that there is no coupling between the final states, so we can treat the transition to each state $|f\rangle$ separately, and the problem reduces to a three-level system. The optical perturbation by the laser beams is given by

$$V(t)=-\boldsymbol{\mu}\cdot\mathrm{Re}[\mathbf{e}_{\mathrm{pump}}e^{-i\omega_{\mathrm{pump}}t}+\mathbf{e}_{\mathrm{probe}}e^{-i\omega_{\mathrm{probe}}t}], \quad \text{(A1)}$$

where $\boldsymbol{\mu}$ is the dipole operator and $\mathbf{e}_{\mathrm{pump}}$, $\mathbf{e}_{\mathrm{probe}}$, ω_{pump}, and ω_{probe} are the electric-field vectors and the frequencies of the pump and the probe beam, respectively. The state of the electron (in the Schrödinger picture) is given by the density operator $\rho(t)$, whose time evolution is described by the Liouville–von Neumann equation[35]

$$\dot{\rho}=-\frac{i}{\hbar}[H_0+V,\rho]+\dot{\rho}_{\mathrm{diss}}. \quad \text{(A2)}$$

Inserting the perturbation V and using the definitions $\tilde{\rho}_{ab}=e^{i(\omega_a-\omega_b)t}\rho_{ab}$, $(\dot{\tilde{\rho}}_{\mathrm{diss}})_{ab}=e^{i(\omega_a-\omega_b)t}(\dot{\rho}_{\mathrm{diss}})_{ab}$, and $V_{ab}=1/\hbar\langle a|V|b\rangle e^{i(\omega_a-\omega_b)t}$ yields

$$\dot{\tilde{\rho}}_{aa}=[-i(V_{ab}\tilde{\rho}_{ba}+V_{ac}\tilde{\rho}_{ca})]+\mathrm{cc.}+(\dot{\tilde{\rho}}_{\mathrm{diss}})_{aa} \quad \text{(A3)}$$

$$\dot{\tilde{\rho}}_{ab} = iV_{ab}(\tilde{\rho}_{aa} - \tilde{\rho}_{bb}) - i(V_{ac}\tilde{\rho}_{cb} - V_{cb}\tilde{\rho}_{ac}) + (\dot{\tilde{\rho}}_{\mathrm{diss}})_{ab}, \tag{A4}$$

with $a \neq b \neq c \neq a$.

V, $\tilde{\rho}$, and $\dot{\tilde{\rho}}_{\mathrm{diss}}$ are Hermitian. Here we only consider the optical transitions from $|i\rangle$ to $|k\rangle$ by the absorption of a pump photon and from $|k\rangle$ to $|f\rangle$ by the absorption of a probe photon (i.e., we exclude one-photon excitation from $|i\rangle$ to $|f\rangle$, and make the rotating-wave approximation). Thus, the only nonvanishing perturbation matrix elements are

$$V_{ik} = \frac{-\boldsymbol{\mu}_{ik}\cdot\mathbf{e}_{\mathrm{pump}}}{2\hbar} e^{i(\omega_i - \omega_k + \omega_{\mathrm{pump}})t} = M_{ik}\cdot e^{i\Omega_{ik}t}, \tag{A5a}$$

$$V_{kf} = \frac{-\boldsymbol{\mu}_{kf}\cdot\mathbf{e}_{\mathrm{probe}}}{2\hbar} e^{i(\omega_k - \omega_f + \omega_{\mathrm{probe}})t} = M_{kf}\cdot e^{i\Omega_{kf}t}, \tag{A5b}$$

and their conjugates, with the shorthand notations M_{ik}, M_{kf}, Ω_{ik}, and Ω_{kf}.

The dissipative term $\dot{\rho}_{\mathrm{diss}}$ in Eq. (A2) describes the energy and phase relaxation on a phenomenological basis. These relaxation processes are mediated by (i) inelastic electron scattering leading to a decay of the population $\tilde{\rho}_{kk}$ in the intermediate state with a rate Γ_k and (ii) quasi-elastic scattering (e.g., with phonons and defects, or the decay of the photohole in $|i\rangle$ to the substrate), which leads to a decay of the coherence between two levels $|a\rangle$ and $|b\rangle$ with the so-called ''pure'' dephasing rate

$$\Gamma^*_{ab} = \Gamma^*_a + \Gamma^*_b. \tag{A6}$$

To keep the number of parameters small, we neglect the energy relaxation in the final state ($\Gamma_f = 0$), and thus obtain for the dissipative terms:

$$(\dot{\tilde{\rho}}_{\mathrm{diss}})_{kk} = -\Gamma_k\tilde{\rho}_{kk} = -(\dot{\tilde{\rho}}_{\mathrm{diss}})_{ii}, \tag{A7.1}$$

$$(\dot{\tilde{\rho}}_{\mathrm{diss}})_{ff} = 0, \tag{A7.2}$$

$$(\dot{\tilde{\rho}}_{\mathrm{diss}})_{ik} = -\left(\Gamma^*_{ik} + \frac{\Gamma_k}{2}\right)\tilde{\rho}_{ik} = -G_{ik}\tilde{\rho}_{ik}, \tag{A7.3}$$

$$(\dot{\tilde{\rho}}_{\mathrm{diss}})_{if} = -\Gamma^*_{if}\tilde{\rho}_{if}, \tag{A7.4}$$

$$(\dot{\tilde{\rho}}_{\mathrm{diss}})_{kf} = -\left(\Gamma^*_{kf} + \frac{\Gamma_k}{2}\right)\tilde{\rho}_{kf} = -G_{kf}\tilde{\rho}_{kf}, \tag{A7.5}$$

where the total dephasing parameters G_{ik} and G_{kf} were introduced to shorten the following equations. To the lowest order in perturbation theory, i.e., neglecting all saturation effects, the Liouville-von-Neumann equation, which is now referred to as optical Bloch equations,[36] thus reduces to:

$$\tilde{\rho}_{ii} \equiv 1, \tag{A8.1}$$

$$\dot{\tilde{\rho}}_{ik} = iM_{ik}\cdot e^{i\Omega_{ik}t}\cdot\tilde{\rho}_{ii} - G_{ik}\tilde{\rho}_{ik}, \tag{A8.2}$$

$$\dot{\tilde{\rho}}_{if} = iM_{kf}\cdot e^{i\Omega_{kf}t}\cdot\tilde{\rho}_{ik} - \Gamma^*_{if}\tilde{\rho}_{if}, \tag{A8.3}$$

$$\dot{\tilde{\rho}}_{kk} = [-i\bar{M}_{ik}\cdot e^{-i\Omega_{ik}t}\cdot\tilde{\rho}_{ik}] + \mathrm{cc.} - \Gamma_k\tilde{\rho}_{kk}, \tag{A8.4}$$

$$\dot{\tilde{\rho}}_{kf} = iM_{kf}\cdot e^{i\Omega_{kf}t}\cdot\tilde{\rho}_{kk} - i\bar{M}_{ik}\cdot e^{-i\Omega_{ik}t}\cdot\tilde{\rho}_{if} - G_{kf}\tilde{\rho}_{kf}, \tag{A8.5}$$

$$\dot{\tilde{\rho}}_{ff} = [-i\bar{M}_{kf}\cdot e^{-i\Omega_{kf}t}\cdot\tilde{\rho}_{kf}] + \mathrm{cc.}, \tag{A8.6}$$

where $\bar{M}_{ik}$ and $\bar{M}_{kf}$ are the complex conjugates of M_{ik} and M_{kf}, respectively. Equations (A8) can easily be integrated to yield[34]

$$\begin{aligned}\dot{\tilde{\rho}}_{ff} = |M_{ik}\cdot M_{kf}|^2 \Bigg[& \frac{4G_{ik}G_{kf}/\Gamma_k - (G_{ik} + \Gamma^*_{if} + G_{kf})}{(G_{ik}^2 + \Omega_{ik}^2)(G_{kf}^2 + \Omega_{kf}^2)} \\ & + \frac{-G_{ik} + \Gamma^*_{if} + G_{kf}}{(G_{ik}^2 + \Omega_{ik}^2)(\Gamma^{*2}_{if} + \Omega_{if}^2)} \\ & + \frac{G_{ik} + \Gamma^*_{if} - G_{kf}}{(\Gamma^{*2}_{if} + \Omega_{if}^2)(G_{kf}^2 + \Omega_{kf}^2)} \\ & + \frac{(G_{ik} + \Gamma^*_{if} - G_{kf})[(\Gamma^*_{if} + G_{kf})^2 - G_{ik}^2]}{(G_{ik}^2 + \Omega_{ik}^2)(\Gamma^{*2}_{if} + \Omega_{if}^2)(G_{kf}^2 + \Omega_{kf}^2)} \Bigg],\end{aligned} \tag{A9}$$

with $\Omega_{if} = \Omega_{ik} + \Omega_{kf}$. The measured 2PPE spectrum $I_{\mathrm{2PPE}}(E_f)$ is proportional to $W_{if} = \dot{\tilde{\rho}}_{ff}$ as a function of the final-state energy E_f, times the product $T(E_f)$ of the density of final states and the transmission function of the spectrometer. Assuming μ_{kf} and Γ^*_f to be independent of E_f, we get

$$\begin{aligned}I_{\mathrm{2PPE}}(\hbar\omega_f) \propto T(\hbar\omega_f)\cdot W_{if}(\hbar\omega_f) = T(\hbar\omega_f)\cdot \frac{|(\boldsymbol{\mu}_{ik}\cdot\mathbf{e}_{\mathrm{pump}})(\boldsymbol{\mu}_{kf}\cdot\mathbf{e}_{\mathrm{probe}})|^2}{8\cdot\hbar^4}\cdot\Bigg[& \frac{2\Gamma^*_{ik}\Gamma^*_{kf}/\Gamma_k + \Gamma^*_k}{(G_{ik}^2 + \Omega_{ik}^2)(G_{kf}^2 + \Omega_{kf}^2)} \\ & + \frac{\Gamma^*_f}{(G_{ik}^2 + \Omega_{ik}^2)(\Gamma^{*2}_{if} + \Omega_{if}^2)} + \frac{\Gamma^*_i + 4\Gamma^*_i\Gamma^*_f(\Gamma^*_i + \Gamma^*_k + \Gamma^*_f + \Gamma_k/2)/(G_{ik}^2 + \Omega_{ik}^2)}{(\Gamma^{*2}_{if} + \Omega_{if}^2)(G_{kf}^2 + \Omega_{kf}^2)}\Bigg],\end{aligned} \tag{A10}$$

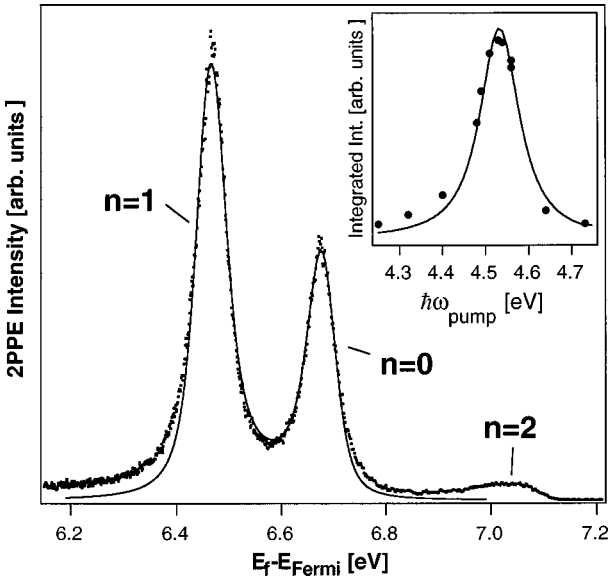

FIG. 6. Main panel: 2PPE spectrum of Cu(111) at 25 K, measured in normal emission ($k_{\parallel}=0$) with $\hbar\omega_{\mathrm{pump}}=4.74$ eV and $\hbar\omega_{\mathrm{probe}}=2.37$ eV (dots). The peaks originate from the occupied $n=0$ surface state and the unoccupied $n=1$ and $n=2$ image potential states. The $n=0$ and $n=1$ peaks were fitted with Eq. (A10) (solid line), convoluted with a Gaussian (FWHM=40 meV) to account for the spectral width of the laser pulses and the spectrometer resolution. Inset: measured (points) and calculated [with Eq. (A10), line] resonance curves, i.e., integrated intensities of the $n=0$ and $n=1$ peaks as a function of the pump-photon energy.

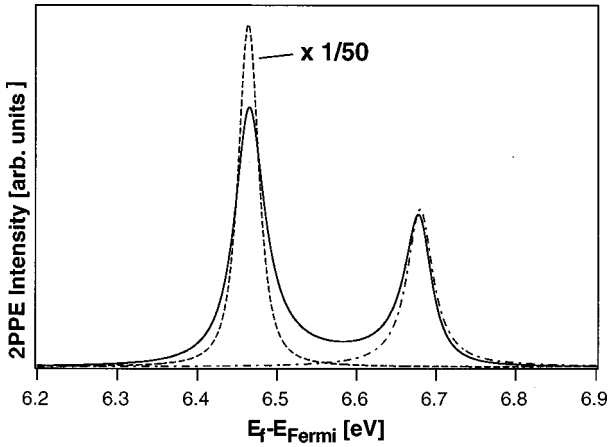

FIG. 7. Influence of the ''pure'' dephasing parameters Γ_i^*, Γ_k^*, and Γ_f^*, and the detuning of the pump beam Ω_{ik} on the 2PPE spectrum, calculated with Eq. (A10). Solid line: fit curve from Fig. 6 without the convolution with the Gaussian. Dashed-dotted line: Same parameters, except for $\Gamma_i^*=\Gamma_k^*=0$ and $\Gamma_f^*=0.03$/fs. Dashed line: Same parameters as the solid line, except $\Omega_{ik}=0$.

where the ω_f dependence lies only in $T(\hbar\omega_f)$, Ω_{kf}, and Ω_{if}. Equation (A10) is the sum of two Lorentz terms and a term proportional to the product of both. The first term in the sum, which is proportional to $1/({G_{kf}}^2+{\Omega_{kf}}^2)$, leads to an ''intermediate state peak'' at the final state energy $E_f=E_k+\hbar\omega_{\mathrm{probe}}$ with a width [full width at half maximum (FWHM)] of $2\hbar G_{kf}$. The second term in the sum, which is proportional to $1/({\Gamma_{if}^*}^2+{\Omega_{if}}^2)$, leads to an ''initial-state peak'' at the final state energy $E_f=E_i+\hbar\omega_{\mathrm{pump}}+\hbar\omega_{\mathrm{probe}}$ with a width (FWHM) of $2\hbar\Gamma_{if}^*$. If the two peaks are well separated, i.e., $\Omega_{ik}\gg G_{kf}+\Gamma_{if}^*$, the last term in the sum, which is proportional to the product of the first and the second term, will also resemble a sum of both Lorentz terms with appropriate constant factors. In this case, the 2PPE spectrum will consist of a Lorentzian ''initial-state peak'' and a Lorentzian ''intermediate-state peak.'' If, on the other hand, the pump beam is in resonance with the transition between $|i\rangle$ and $|k\rangle$, i.e., $\Omega_{ik}=0$, the multiplication of the two Lorentzian denominators in the last term of Eq. (A10) will cause a linewidth narrowing of the resonance peak. At the same time the $1/({G_{ik}}^2+{\Omega_{ik}}^2)$ factors will lead to a resonance enhancement.

Figure 6 (main panel) shows a 2PPE spectrum of Cu(111) at 25 K measured in normal emission ($k_{\parallel}=0$) with two 80-fs laser pulses with $\hbar\omega_{\mathrm{pump}}=4.74$ eV, and $\hbar\omega_{\mathrm{probe}}=2.37$ eV (dots).[10] The spectrum shows three peaks that originate from the occupied $n=0$ surface state and the unoccupied $n=1$ and $n=2$ image-potential states. The $n=0$ and $n=1$ peaks were fitted with Eq. (A10) (solid line), setting the lifetime of the $n=1$ state ($1/\Gamma_k$) to the measured value of 22 fs.[10] The calculated curve was convoluted with a Gaussian function (FWHM=40 meV) to account for the spectral width of the laser pulses and the spectrometer resolution. The measured spectrum is very well fitted by the pure dephasing parameters $\Gamma_i^*=0.031$/fs, $\Gamma_k^*=0.012$/fs, and $\Gamma_f^*=0$. The inset of Fig. 6 shows the measured (points) and calculated (line) resonance curves, i.e., the integrated intensities of the $n=0$ and the $n=1$ peak as a function of the pump-photon energy. Again, the measurements are well reproduced by Eq. (A10). This shows that 2PPE from the $n=0$ and the $n=1$ state can be described as a single direct excitation process, which leads to two peaks as a consequence of ''pure'' dephasing in the initial and the intermediate states.

If there is no ''pure'' dephasing in the initial and the intermediate state, i.e., $\Gamma_i^*=\Gamma_k^*=0$, the transition rate W_{if} from Eq. (A10) reduces to

$$W_{if}(\hbar\omega_f)=\frac{|(\boldsymbol{\mu}_{ik}\cdot\mathbf{e}_{\mathrm{pump}})(\boldsymbol{\mu}_{kf}\cdot\mathbf{e}_{\mathrm{probe}})|^2}{8\cdot\hbar^4}\cdot\times\frac{\Gamma_f^*}{[(\Gamma_k/2)^2+\Omega_{ik}^2]({\Gamma_f^*}^2+\Omega_{if}^2)},\quad\text{(A11)}$$

which leads to a spectrum consisting of a single Lorentzian ''initial state peak'' and no ''intermediate state peak.'' This case is shown by the dashed-dotted line in Fig. 7 which is calculated with the same parameters as the fit curve in Fig. 6, except for $\Gamma_i^*=\Gamma_k^*=0$ and $\Gamma_f^*=0.03$/fs. For comparison, the solid line in Fig. 7 repeats the fit curve from Fig. 6 without the convolution with the Gaussian function. The dashed line in Fig. 7 shows the case that the pump beam is in resonance with the transition between $|i\rangle$ and $|k\rangle$, in this case $\hbar\omega_{\mathrm{pump}}=4.52$ eV. The other parameters are the same as for the solid line. A strong resonance enhancement and a pronounced narrowing of the peak are clearly visible, as was also observed by Wallauer and Fauster[30] and calculated by Ueba.[37]

B. 2PPE from one initial state, several intermediate states

Next we consider the scenario of 2PPE from a discrete initial state $|i\rangle$ via several intermediate states $|k\rangle$, where k is now an index variable. In this case, the contributions from the different intermediate states interfere. This scenario applies, e.g., to the Cu(111) surface when the higher image potential states ($n=2,3,...$) are taken into account (however, the contribution of the $n=1$ state usually dominates, see Fig. 6). Höfer *et al.*[7] found fascinating interference effects of the higher image states on Cu(100) in time-resolved 2PPE with ultrashort (i.e., spectrally broad) laser pulses. Note, however, that on Cu(100) the excitation starts from a continuum of initial states.

We neglect the coupling between the intermediate states, and restrict ourselves to the case of vanishing ''pure'' dephasing in the initial and the intermediate states ($\Gamma_i^*=0$, $\Gamma_k^*=0\forall k$). Then Eq. (A11) is generalized to

$$W_{if}(\hbar\omega_f)=\left|\sum_k \frac{(\boldsymbol{\mu}_{ik}\cdot\mathbf{e}_{\text{pump}})(\boldsymbol{\mu}_{kf}\cdot\mathbf{e}_{\text{probe}})}{\Gamma_k/2+i\Omega_{ik}}\right|^2 \frac{\Gamma_f^*/(8\hbar^4)}{\Gamma_f^{*2}+\Omega_{if}{}^2}. \tag{A12}$$

Note that Eq. (A12), like Eq. (A11), leads to a spectrum with a single Lorentzian ''initial state peak'' with a FWHM of $2\hbar\Gamma_f^*$. In 2PPE from a single initial state, ''intermediate state peaks'' will appear only if there is ''pure'' dephasing in the initial or the intermediate states. This is a consequence of energy conservation.

C. 2PPE from a continuum of initial states

If there are several initial states $|i\rangle$ (i is now an index variable, too), which do not interact among themselves, their signals add up to the measured 2PPE spectrum:

$$I_{\text{2PPE}}(\hbar\omega_f)\propto T(\hbar\omega_f)\cdot\sum_i W_{if}(\hbar\omega_f). \tag{A13}$$

A special case, which was also treated by Ueba,[37] is formed by a continuum of initial states with a constant density D_i, where the dipole-matrix elements μ_{ik} and the relaxation rates Γ_i^* and Γ_k do not depend on the initial-state energy E_i. Again we restrict ourselves to the case of vanishing dephasing in the initial and intermediate states ($\Gamma_i^*=\Gamma_k^*=0\forall i,k$). Then $I_{\text{2PPE}}(\hbar\omega_f)\propto T(\hbar\omega_f)\cdot W(\hbar\omega_f)$ with

$$W(\hbar\omega_f)=\frac{D_i\Gamma_f^*}{8\hbar^4}\int\left|\sum_k \frac{(\boldsymbol{\mu}_{ik}\cdot\mathbf{e}_{\text{pump}})(\boldsymbol{\mu}_{kf}\cdot\mathbf{e}_{\text{probe}})}{\Gamma_k/2+i(\omega_i-\omega_k+\omega_{\text{pump}})}\right|^2 \times\frac{d(\hbar\omega_i)}{\Gamma_f^{*2}+(\omega_i-\omega_f+\omega_{\text{probe}}+\omega_{\text{pump}})^2}, \tag{A14}$$

and with the substitution $\omega=\omega_i-\omega_f+\omega_{\text{pump}}+\omega_{\text{probe}}$

$$W(\hbar\omega_f)=\frac{D_i\Gamma_f^*}{8\hbar^3}\int\left|\sum_k \frac{(\boldsymbol{\mu}_{ik}\cdot\mathbf{e}_{\text{pump}})(\boldsymbol{\mu}_{kf}\cdot\mathbf{e}_{\text{probe}})}{\Gamma_k/2-i(\Omega_{kf}-\omega)}\right|^2\cdot\frac{d\omega}{\Gamma_f^{*2}+\omega^2}. \tag{A15}$$

The spectrum consists of interfering Lorentzian ''intermediate state peaks'' with FWHM's of $\hbar\Gamma_k$, convoluted with a Lorentz curve with a FWHM of $2\hbar\Gamma_f^*$. If $\Gamma_f^*\ll\Gamma_k\forall k$, Eq. (A15) reduces to

$$W(\hbar\omega_f)=\frac{\pi D_i}{8\hbar^3}\left|\sum_k \frac{(\boldsymbol{\mu}_{ik}\cdot\mathbf{e}_{\text{pump}})(\boldsymbol{\mu}_{kf}\cdot\mathbf{e}_{\text{probe}})}{\Gamma_k/2-i\Omega_{kf}}\right|^2. \tag{A16}$$

Thus, with a continuum of initial states [like, e.g., in the excitation of image potential states on Cu(100)], ''pure'' dephasing is not necessary for ''intermediate state peaks.''[7]

D. Density of final states and spectrometer transmission function

The measured 2PPE spectrum is proportional to the product $T(E_f)$ of the density of final states and the transmission function of the spectrometer. The latter depends on the geometry of the experiment, in particular on the electric fields between the sample and the spectrometer. An idealized situation is that the region between the sample and the spectrometer is kept field free, and the spectrometer accepts all photoemitted electrons within a certain solid angle $\Delta\Omega$ (which may, e.g., be defined by the spot of the laser beams on the surface and the entrance aperture of the spectrometer), where $\Delta\Omega$ does not depend on the kinetic energy $E_{\text{kin}}=E_f-E_{\text{vac}}$ of the electrons. Then $T(E_f)$ is proportional to the number of free-electron states within $\Delta\Omega$, which lie in a small energy interval $[E_f,E_f+\Delta E_f]$. Since the density of free-electron states is constant in k space,

$$T(E_f)\propto\Delta\Omega\cdot k_f{}^2\cdot\left.\frac{1}{dE/dk}\right|_{k_f} \tag{A17.1}$$

with

$$k_f=\frac{\sqrt{2m_e\cdot E_{\text{kin}}}}{\hbar}=\frac{\sqrt{2m_e(E_f-E_{\text{vac}})}}{\hbar} \tag{A17.2}$$

and

$$\left.\frac{dE}{dk}\right|_{k_f}=\frac{\hbar^2k_f}{m_e}. \tag{A17.3}$$

Thus,

$$T(E_f)\propto\Delta\Omega\cdot k_f\propto\Delta\Omega\cdot\sqrt{E_{\text{kin}}}=\Delta\Omega\cdot\sqrt{E_f-E_{\text{vac}}}. \tag{A18}$$

If a negative-bias voltage U_{bias} is applied to the sample (i.e., the electrons are accelerated towards the spectrometer), the acceptance angle of the spectrometer will increase for all photoemitted electrons, but more for the slow electrons. Thus, the contribution of low-energy electrons to the measured spectrum will increase. On the other hand, if a *positive* bias voltage is applied to the sample, the contribution of low-energy electrons to the measured spectrum will decrease (even to zero for $E_f<E_{\text{vac}}+eU_{\text{bias}}$).

[1] J. Bokor, Science **246**, 1130 (1989).
[2] R. Haight, Surf. Sci. Rep. **21**, 275 (1996).
[3] W. Steinmann, Appl. Phys. A: Solids Surf. **A49**, 365 (1989).
[4] T. Fauster and W. Steinmann, in *Electromagnetic Waves: Recent Development in Research*, edited by P. Halevi (Elsevier, Amsterdam, 1995), p. 350.
[5] C. B. Harris, N.-H. Ge, R. L. Lingle, Jr., J. D. McNeill, and C. M. Wong, Annu. Rev. Phys. Chem. **48**, 711 (1997).
[6] M. Wolf, Surf. Sci. **377-379**, 343 (1997).
[7] U. Höfer, I. L. Shumay, C. Reuß, U. Thomann, W. Wallauer, and T. Fauster, Science **277**, 1480 (1997).
[8] H. Petek, A. P. Heberle, W. Nessler, H. Nagano, S. Kubota, N. Matsunami, N. Moriya, and S. Ogawa, Phys. Rev. Lett. **78**, 4649 (1997).
[9] H. Petek and S. Ogawa, Prog. Surf. Sci. **56**, 239 (1998).
[10] E. Knoesel, A. Hotzel, and M. Wolf, J. Electron Spectrosc. Relat. Phenom. **88-91**, 577 (1998).
[11] M. Aeschlimann, M. Bauer, S. Pawlik, W. Weber, R. Burgermeister, D. Oberli, and H. C. Siegmann, Phys. Rev. Lett. **79**, 5158 (1997).
[12] T. Hertel, E. Knoesel, A. Hotzel, M. Wolf, and G. Ertl, J. Vac. Sci. Technol. A **15**, 1503 (1997).
[13] S. Ogawa, H. Nagano, H. Petek, and A. P. Heberle, Phys. Rev. Lett. **78**, 1339 (1997).
[14] X.-Y. Zhu, J. M. White, M. Wolf, E. Hasselbrink, and G. Ertl, Chem. Phys. Lett. **176**, 459 (1991).
[15] L. J. Richter, S. A. Buntin, D. S. King, and R. R. Cavanagh, Chem. Phys. Lett. **186**, 423 (1991).
[16] M. Wolf, X.-Y. Zhu, and J. M. White, Chem. Phys. Lett. **196**, 422 (1992).
[17] Y. Matsumoto, Y. A. Gruzdkov, K. Watanabe, and K. Sawabe, J. Chem. Phys. **105**, 4775 (1996).
[18] E. Knoesel, D. Velic, A. Hotzel, M. Wolf, H. Over, G. Ertl, L. Bartels, T. Klamrot, and P. Saalfrank (unpublished).
[19] T. Hertel, E. Knoesel, E. Hasselbrink, M. Wolf, and G. Ertl, Surf. Sci. **317**, L1147 (1994).
[20] E. Knoesel, T. Hertel, M. Wolf, and G. Ertl, Chem. Phys. Lett. **240**, 409 (1995).
[21] L. Bartels, G. Meyer, H. Rieder, D. Velic, E. Knoesel, A. Hotzel, M. Wolf, and G. Ertl, Phys. Rev. Lett. **80**, 2004 (1998).
[22] S. Hüfner, *Photoelectron Spectroscopy* (Springer, Berlin, 1995).
[23] W. Demtröder, *Laser Spectroscopy* (Springer, Berlin, 1996).
[24] J. D. E. McIntyre, in *Advances in Electrochemistry and Electrochemical Engineering*, edited by P. Delahay and C. W. Tobias (Wiley, New York, 1973), p. 61.
[25] H. Behrens and G. Ebel, *Physik Daten* (Fachinformationszentrum, Karlsruhe, 1981), Vol. 18.
[26] P. J. Feibelman, Prog. Surf. Sci. **12**, 287 (1982).
[27] E. W. Plummer and W. Eberhardt, Adv. Chem. Phys. **49**, 533 (1982).
[28] F. M. Zimmermann and W. Ho, Surf. Sci. Rep. **22**, 127 (1995).
[29] R. Raval, S. F. Parker, M. E. Pemble, P. Hollins, J. Prichard, and M. A. Chesters, Surf. Sci. **203**, 353 (1988).
[30] W. Wallauer and T. Fauster, Surf. Sci. **374**, 44 (1997).
[31] E. Knoesel, A. Hotzel, and M. Wolf, Phys. Rev. B **57**, 12 812 (1998).
[32] K. D. Tsuei and P. D. Johnson, Phys. Rev. B **45**, 13 827 (1992).
[33] C. Reuß, I. L. Shumay, U. Thomann, M. Kutschera, M. Weinelt, T. Fauster, and U. Höfer, Phys. Rev. Lett. **82**, 153 (1999).
[34] V. S. Letokhov and V. P. Chebotayev, *Nonlinear Laser Spectroscopy* (Springer-Verlag, Berlin, 1977).
[35] K. Blum, *Density Matrix Theory and Applications* (Plenum, New York, 1981).
[36] R. Loudon, *The Quantum Theory of Light* (Oxford University Press, New York, 1983).
[37] H. Ueba, Surf. Sci. **334**, L719 (1995).